Time-resolved atomic inner-shell spectroscopy

M. Drescher*†**, M. Hentschel*****, R. Kienberger*****, M. Uiberacker*****, V. Yakovlev*****, A. Scrinzi*****, Th. Westerwalbesloh**†**, U. Kleineberg**†**, U. Heinzmann**† **& F. Krausz***

* *Institut für Photonik, Technische Universität Wien, Gusshausstrasse 27, A-1040 Wien, Austria*
† *Fakultät für Physik, Universität Bielefeld, Universitätsstrasse 25, D-33615 Bielefeld, Germany*

....

The characteristic time constants of the relaxation dynamics of core-excited atoms have hitherto been inferred from the linewidths of electronic transitions measured by continuous-wave extreme ultraviolet or X-ray spectroscopy. Here we demonstrate that a laser-based sampling system, consisting of a few-femtosecond visible light pulse and a synchronized sub-femtosecond soft X-ray pulse, allows us to trace these dynamics directly in the time domain with attosecond resolution. We have measured a lifetime of $7.9^{+1.0}_{-0.9}$ fs of M-shell vacancies of krypton in such a pump–probe experiment.

Many-body systems with excess internal energy relax towards states of lower energy by rearrangement of molecular, atomic or nuclear structure. Observing these processes in real time requires a pump pulse for initiating the microscopic dynamics and a delayed probe pulse for detecting transition states of the evolving system. Time-resolved spectroscopy based upon this pump–probe approach[1] is now routinely used for tracking atomic motion in molecules with femtosecond laser pulses[2].

Electronic motion in weakly bound (Rydberg) states can also be captured with optical or infrared pulses[3]. However, the relaxation dynamics of core-excited atoms is out of the reach of femtosecond optical techniques. Excitation of a strongly bound electron from an atomic inner shell is followed by an ultrafast rearrangement of the electronic system, resulting in a disappearance of the inner-shell vacancy (henceforth briefly referred to as core hole). Characteristic time constants of the concomitant electronic dynamics range from a few attoseconds ($1\,\text{as} = 10^{-18}\,\text{s}$) to a few femtoseconds depending on the energy of the core hole and the strength of electronic coupling.

The lifetime of core holes can be inferred from the energy spectral width of the photons or electrons emitted upon the decay of the excited atomic state. However, except for specific cases of isolated resonances without incoherent background, energy-domain measurements on their own are—in general—unable to provide detailed and accurate insight into the evolution of multi-electron dynamics. As a complementary technique, time-domain access would be desirable. Time-resolved spectroscopy of core-excited atoms calls for several new tools and techniques. The core hole must be created within a time interval that is short compared to its decay time: that is, within typically less than 1 femtosecond. Sampling of the subsequent atomic relaxation calls for a synchronized probe pulse and for a suitable probing technique.

The recent demonstration of isolated sub-femtosecond soft-X-ray pulses[4,5] and trains of pulses[6,7] along with attosecond sampling of photo-electron wave packets with a few-cycle optical wave[5,8] opened the door to attosecond atomic spectroscopy[9]. Here we use these tools and techniques to track rearrangement of the electronic system of a core-excited atom. The core hole is created within less than a femtosecond and its subsequent decay can be observed on a few-femtosecond timescale. The applied technique offers attosecond resolution and will allow time-resolved spectroscopy of a wide range of atomic processes.

Decay of atomic core holes

Excitation of an electron from an atomic shell other than the outermost valence orbital by the impact of an energetic particle—for example, a photon or electron (here we use photons)—creates a transient hole state of energy W_h (see process a in Fig. 1a). This core hole is not stable, so the system tends to minimize its energy by filling the vacancy with an electron from an outer shell (see process b in Fig. 1a). The excess binding energy $W_h - W_1$ is either carried away by an extreme ultraviolet or X-ray fluorescence photon or transferred via electrostatic forces to another (Auger) electron, which subsequently escapes from the atomic binding (see process c in Fig. 1a). The latter relaxation channel is most probable for light atoms and moderate binding energies ($W_h < 1\,\text{keV}$) but remains intact for $W_h > 1\,\text{keV}$ (ref. 10).

Owing to several Auger relaxation channels, the energy spectrum of the ejected electrons usually contains a number of Auger lines. Further, several photo lines originating from atomic shells with binding energy smaller than the energy of the exciting X-ray photon, $\hbar\omega_X$, add to the spectrum. In Fig. 1a just a single Auger line and a couple of photo lines represent this manifold. The mean kinetic energy of the Auger electron $W_{kin} = W_h - W_1 - W_2$ and its spectral width Γ are fully determined by intrinsic atomic properties. By contrast, the photo electrons carry the energy of the absorbed photon diminished by their atomic binding energy and hence—in the absence of resonances—their energy distribution reflects that of the exciting radiation.

The feasibility of time-resolved inner-shell spectroscopy relies on X-ray pulses with a duration τ_X much shorter than the lifetime of the generated core hole τ_h. Under these circumstances the temporal evolution of the production rate dN/dt or—in the language of quantum mechanics—the temporal shape $|\psi(t)|^2$ of the ejected wave packet is very different for photo and Auger electrons (Fig. 1b). If the photo-ionization cross-section is nearly constant within the bandwidth of the X-ray pulse, $|\psi_{photo}(t)|^2$ follows the temporal profile of the exciting X-ray pulse $|E_X(t)|^2$ and thus the production rate of core holes. For $\tau_X \ll \tau_h$, the front edge of $|\psi_{Auger}(t)|^2$ rises within τ_X, whereas its trailing edge tracks the decay of the core holes. Thus, sampling the time evolution of photo and Auger electron emission explores the generation and decay of core-excited atoms in real time.

Sampling electron emission with light

Strong-field physics provides the key to trace electron emission from atoms. The presence of a strong light field affects the ejected electrons' motion and can be used to probe the emission. Assuming a linearly polarized few-cycle probe light field $E_L(t) = E_a(t)\cos(\omega_L t + \varphi)$, the final momentum (reached after the light pulse left the interaction volume) of an electron released at the

instant t_r is changed by $\Delta p(t_r) = [eE_a(t_r)/\omega_L]\sin(\omega_L t_r + \varphi)$ along the light electric field vector according to a simple classical analysis[4] (Fig. 2a). E_a is the amplitude envelope, and ω_L and φ stand for the carrier frequency and carrier-envelope phase of the laser pulse, respectively. The final energy is given by:

$$W_f(t_r) = W_i + 2U_p(t_r)\sin^2(\omega_L t_r + \varphi)\cos 2\theta$$

$$+ [8W_i U_p(t_r)]^{1/2}\sin(\omega_L t_r + \varphi)\cos\theta \qquad (1)$$

where $U_p(t) = e^2 E_a^2(t)/4m_e\omega_L^2$ is the electron's cycle-averaged quiver energy in the probe light field, e, m_e and W_i are the electron's charge, mass and initial energy, and θ is the angle between its final momentum vector and the light electric field vector. For $\theta \approx 0°$ (Fig. 2b) and $W_i \gg \hbar\omega_L$, a moderate field strength ($U_p \approx \hbar\omega_L$) is able to shift the electron energy by many electronvolts. The energy shift varies from zero to its maximum value within a quarter-wave cycle $T_0/4 = \pi/2\omega_L$ (≈ 0.6 fs at $\lambda_L = 750$ nm). This time-to-energy mapping permits sampling of electron emission with attosecond resolution. The final energy spectrum for an initial energy distribution $dN/dW = f_W(W_i)$ and time structure $dN/dt = f_t(t_r - t_{r0})$, where t_{r0} represents the instant of the emission peak, can be calculated for any detection direction θ and timing t_{r0} by using equation (1). Experimentally, t_{r0} can be varied by varying the arrival time, that is, the delay Δt (Fig. 2b), of the probe light pulse relative to the X-ray pump pulse that triggers the electron emission. For large initial kinetic energy, $W_i \gg \hbar\omega_L$, the validity of this simple classical treatment of the influence of a strong light field on electrons emitted within a fraction of the light wave cycle T_0 has been corroborated by several photo-emission experiments[5,8] as well as by quantum mechanical analyses[11,12].

We have generalized one (ref. 12) of these quantum theories addressing photo-electron emission in the presence of a strong laser field to describe the behaviour of Auger electrons emitted under similar conditions (for more details see Supplementary Information). Our theory yields the temporal evolution of hypothetical single-line Auger electron spectra probed by strong few-cycle light for different decay times τ_h as shown in Fig. 3. In our modelling we assumed $\tau_X = 0.5$ fs (at $\hbar\omega_X = 100$ eV) and $\tau_L = 5$ fs (at $\lambda_L = 750$ nm, $\hbar\omega_L \approx 1.6$ eV), corresponding to the current state of the art. For $\tau_h < T_0/2$ (Fig. 3a–c), the energy distribution of the Auger electrons exhibits pronounced variation as the delay Δt is varied by as little as $T_0/4$ (for $\tau_h \lesssim T_0/5$ in close agreement with the results of the above classical treatment). From the energy distributions recorded for different values of Δt, the temporal evolution
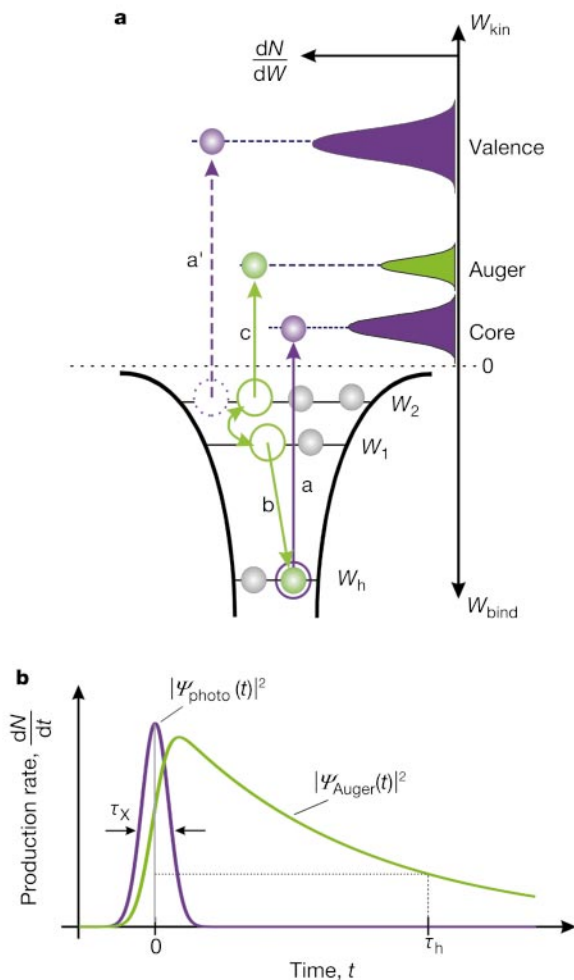
Figure 1 Schematic illustration of atomic excitation and relaxation processes following exposure to an ultrashort X-ray pulse. **a**, In the absence of resonances, the atom instantly responds by ejecting photo electrons (processes a, a′) with $|\psi_{photo}(t)|^2$ following the temporal intensity profile of the exciting X-ray pulse. The inner-shell vacancy (W_h) is subsequently filled (process b) by an electron from an outer shell upon emission (process c) of a secondary (Auger) electron with $|\psi_{Auger}(t)|^2$ tracing the decay of the inner-shell vacancy. **b**, Probing the emitted photo and Auger electrons reveals the excitation and relaxation dynamics of core-excited atoms. W_{kin}, kinetic energy; W_{bind}, binding energy; W_h, $W_{1,2}$, binding energies of core and valence electrons, respectively; N, number of freed electrons. τ_X, duration of X-ray pulse; τ_h, decay time of core hole. The photo and Auger electrons are represented here (as in Fig. 5) in violet and green, respectively.
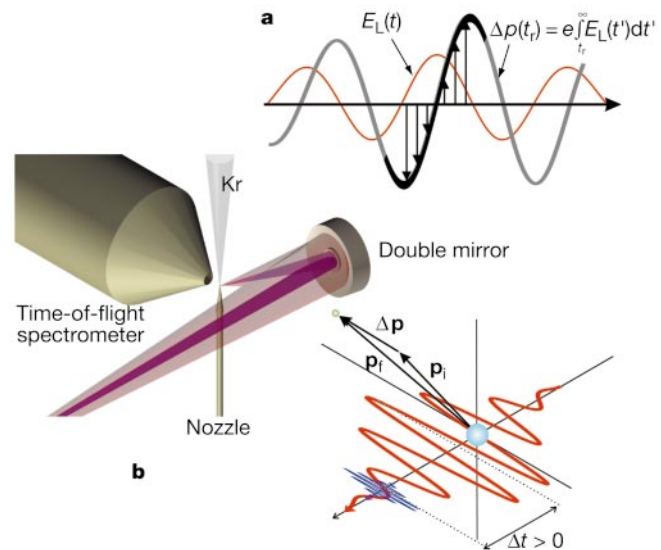
Figure 2 Attosecond two-colour sampling technique for probing electron emission from atoms. An extreme ultraviolet or X-ray pulse excites the atomic target and induces electron emission (see Fig. 1a). A delayed probe light pulse transfers a momentum Δp to the ejected electron after its release. p_i and p_f represent the electron's initial and final momentum, respectively. **a**, The transferred momentum sensitively depends on the phase and amplitude of the light field vector $E_L(t)$ at the instant of release resulting in a time-to-energy mapping on an attosecond timescale. For processes lasting less than the light cycle the oscillating light field constitutes a sub-femtosecond probe, whereas processes lasting longer than the light-wave cycle are sampled by the amplitude envelope of the laser pulse. In both cases, a sequence of light-affected electron energy spectra are recorded at different delays Δt, from which the time evolution of electron emission is reconstructed. **b**, In our experiments, we used a 97-eV, sub-femtosecond soft-X-ray pulse for excitation and a 750-nm (1.6 eV), sub-7-fs few-cycle light pulse for probing electron emission. The two pulses are collinearly focused into a krypton gas target by a two-component mirror similar to that used in ref. 5 but designed to reflect photons with higher energies. The kinetic energy distribution of the ejected photo and Auger electrons has been measured with a time-of-flight spectrometer aligned parallel to the polarization direction of the light pulse and the X-ray pulse.

of both the emission rate and a possible energy sweep of the electrons may be retrieved with a resolution of about $T_0/20$ (≈ 100 as at $\lambda_L = 750$ nm) in future studies of sub-femtosecond inner-shell dynamics.

For τ_h approaching and exceeding T_0 (Fig. 3c–e), which is relevant to our current experiment, variation of the energy distribution with Δt within the laser cycle gradually disappears. The energy spectrum is broadened and broken up into sidebands spaced by $\hbar\omega_L$ at any Δt within the range of temporal overlap of electron emission and the laser pulse[13–16]. The sidebands originate from quantum interferences between different portions of the ejected electron wave packet experiencing the same momentum shift by the laser field. Although the overall width of the broadened energy distribution can still be estimated from the classical treatment, the emergence of the sideband structure can only be accounted for by quantum models. For electron emission times comparable to or longer than T_0 (Fig. 3d, e) the number of electrons scattered into sidebands is predicted to be proportional to the convolution of electron emission and the laser pulse. Hence for dynamics extending over T_0 or longer, evaluation of the X-ray-pump/visible-light-probe experiments does not rely on the energy–time mapping (in equation (1)) required for sub-cycle dynamics. Rather, the sideband area versus Δt directly yields the temporal evolution of electron emission (by deconvolution), provided that the laser pulse is sufficiently short (a few femtoseconds) in duration.

Recently we applied this general concept to sampling photo-electron emission with a few-cycle probe light pulse. From the measured photo-electron emission time we obtained the duration of the ionizing soft-X-ray pulse[5,8]. The measurements revealed that few-cycle light-driven atoms are capable of emitting isolated soft-X-ray pulses ($\hbar\omega_X \approx 100$ eV) with sub-femtosecond duration ($\tau_X < 0.5$ fs) in excellent synchrony ($\Delta t_{jitter} < 0.2$ fs) with the phase of its few-cycle ($\tau_L \approx 7$ fs) driver light wave[8]. These pulses,

along with the above concept for electron sampling, combine to give an attosecond-resolution pump–probe technique for tracing electron dynamics after core-level excitation of atoms (or molecules).

Tracing the decay of an M-shell vacancy in krypton

For the first proof-of-principle experiments we selected one of the most comprehensively studied atomic inner-shell relaxation processes, the MNN Auger decay in krypton[17–20]. The Lorentz-type line profiles of the resultant Auger electrons imply an exponential decay of the core hole with a few-femtosecond lifetime. Using the notation of Fig. 1, in this case W_h, W_1 and W_2 correspond to the $3d$, $4s$ and $4p$ sub-shells, respectively.

The pump–probe apparatus used here has been described elsewhere[5]. Briefly, the few-cycle light pulse ($\tau_L \approx 7$ fs, $\lambda_L = 750$ nm, $T_0 = 2.5$ fs) is delivered in an annular beam and hits the outer part of the two-component mirror shown in Fig. 2b. The soft-X-ray pulse with a continuum spectrum extending to photon energies of around 100 eV (ref. 8) propagates in a collinear beam matching the diameter of the inner part of the two-component mirror. For the current experiments, a dedicated Mo/Si multilayer mirror with a reflectance curve peaking at 97 eV has been manufactured. The energy spectrum of the X-ray pulse filtered by the mirror was upshifted as compared to previous experiments[5,8] to avoid the excitation of $3d$ electrons into Rydberg states, which comes into play at $\hbar\omega_X < 95$ eV. The energy upshift comes at the expense of a narrower bandwidth of the Mo/Si multilayer (full-width at half-maximum, FWHM ≈ 3 eV), resulting in an increased pulse duration, $\tau_X \approx 0.9$ fs, as compared to recent experiments[5,8].

Both the X-ray and the light pulse are polarized along the axis of the time-of-flight electron energy spectrometer (Fig. 2b) to collect the electrons with a final momentum directed nearly parallel to the laser polarization. This parallel detection geometry is characterized by $\theta \approx 0°$ and 'activates' the last term in equation (1). A comparison
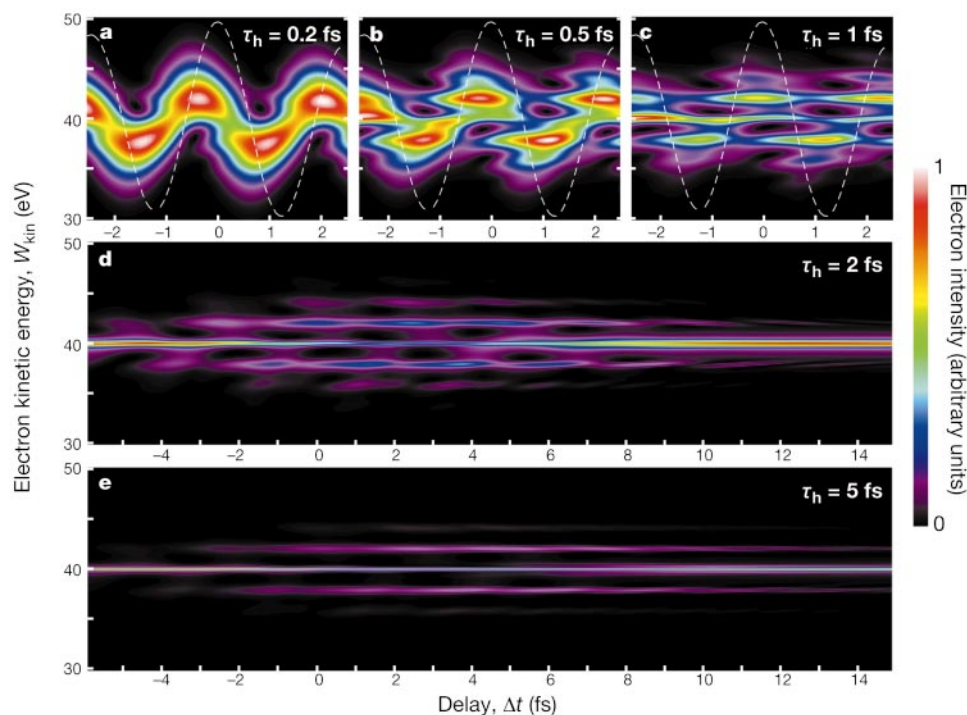
Figure 3 Laser sampling of Auger electron emission with attosecond resolution. Simulated electron spectra of a single isolated Auger line resulting from a hypothetical atomic core hole decay of different decay time constants τ_h in the presence of a few-cycle 750-nm laser field ($T_0 = 2.5$ fs) with $\varphi \approx 0$ using our quantum mechanical model (Supplementary Information). The spectra are shown in false-colour representation at small delays near $\Delta t = 0$ for sub-femtosecond decays (**a**, **b**, **c**) and over an extended delay range for decays lasting longer than the wave cycle (**d**, **e**). The dashed line represents the laser electric field. The durations of the exciting X-ray and probing laser pulse and the peak intensity of the latter were assumed to be $\tau_X = 0.5$ fs, $\tau_L = 5$ fs (FWHM) and $I_p = 5 \times 10^{11}$ W cm^{-2}, respectively.
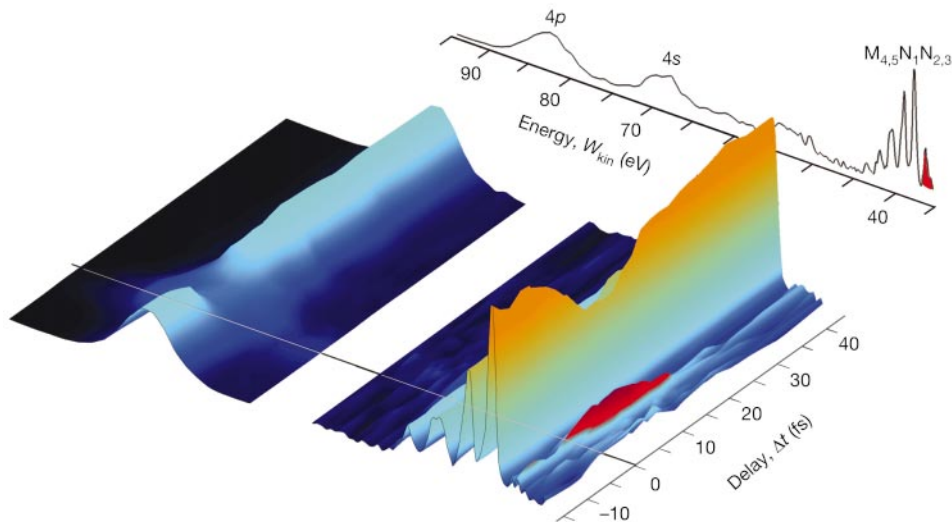
Figure 4 Evolution of electron spectra following core excitation. The spectra were recorded after the exposure of krypton atoms to a 97-eV sub-femtosecond X-ray pulse and a sub-7-fs, 750-nm laser pulse at different delays between the pulses. The surface plot shows the evolution of the $4p$ photo line and the $M_{4,5}N_1N_{2,3}$ Auger lines with Δt. The spectrum highlighted in the background was recorded at $\Delta t = 5$ fs. According to equation (1) the kinetic energy spectrum of the sub-laser-cycle-duration photo electrons ($4s$ and $4p$ lines) should be periodically shifted versus Δt. However, for τ_X comparable to $T_0/2$ this periodic shift merges to a continuous broadening (probing the laser amplitude

envelope $E_a(t)$) owing to the absence of stabilization of the absolute phase φ in our laser pulses, because light pulses with $\varphi \approx 0$ and $\varphi \approx \pi$ induce shifts of opposite sign and turn asymmetric shifts into symmetric broadening. The laser peak intensity was evaluated from the broadening of photo lines as $I_p \approx 5 \times 10^{11}$ W cm^{-2}. The evolution of the first-order sideband (highlighted in red) of the lowest-energy member of the $M_{4,5}N_1N_{2,3}$ Auger group reflects the delayed decay dynamics of the krypton $3d$ core hole. A pronounced positive temporal shift of the side-band maximum with respect to the photo-line minimum is clearly discernible (see also Fig. 5).

of the second and third terms in equation (1) reveals that, for $W_i \gg \hbar\omega_L$, this results in a detectable change of the electron energy at substantially lower light-field strengths compared to the orthogonal detection geometry ($\theta \approx 90°$). The low field strength helps to avoid both multiphoton ionization and a perturbation to the studied electronic relaxation. The experimental results are summarized in a surface plot compiled from 20 spectra recorded at a sequence of pump–probe delays Δt (defined in Fig. 2b), each one integrated over 300,000 laser shots and normalized to constant integral electron counts (Fig. 4). By definition, $\Delta t = 0$ at the coincidence of the peaks of the X-ray and laser pulses, which has been experimentally determined by observing the maximum broadening of the $4p$ and $4s$ photo lines.

The improved transmittivity and spectral resolution (~ 0.5 eV) of the time-of-flight spectrometer at lower kinetic energies favours the $M_{4,5}N_1N_{2,3}$ Auger group around 40 eV for an in-depth analysis. Before doing this we can make a few instructive observations. The photo lines are broadened smoothly (without the appearance of sidebands) in the range of temporal overlap between the laser and the X-ray pulse, indicating the sub-T_0 duration of the emitted electron wave packet (for more detailed comments, see legend of Fig. 4). In strong contrast, the Auger lines do not exhibit notable broadening. Instead, they are redistributed into sidebands spaced by $\hbar\omega_L \approx 1.6$ eV under the influence of the laser field. This is indicative of an Auger emission time comparable to or longer than T_0 according to our above discussion. The conspicuous suppression of the most prominent Auger peak and the simultaneous appearance of its first-order sideband (highlighted in red; other sidebands are hidden in the MNN group) indeed survive the broadening of the photo lines (for $\Delta t > 0$), confirming prolonged emission of the Auger electrons compared to that of photo-electrons.

For a quantitative analysis of the Auger emission we evaluated the sideband area A_{sb} (highlighted in red in Fig. 4) from the normalized electron spectra by combined gaussian peak-fitting to the whole $M_{4,5}N_1N_{2,3}$ group. The evolution of $A_{sb}(\Delta t)$ is shown by the circles in Fig. 5a. Figure 5b depicts the broadening $\delta w(\Delta t) = [\Delta w(\Delta t)^2 - \Delta w(\infty)^2]^{1/2}$ of the width Δw of the $4p$ photo line (circles) recorded
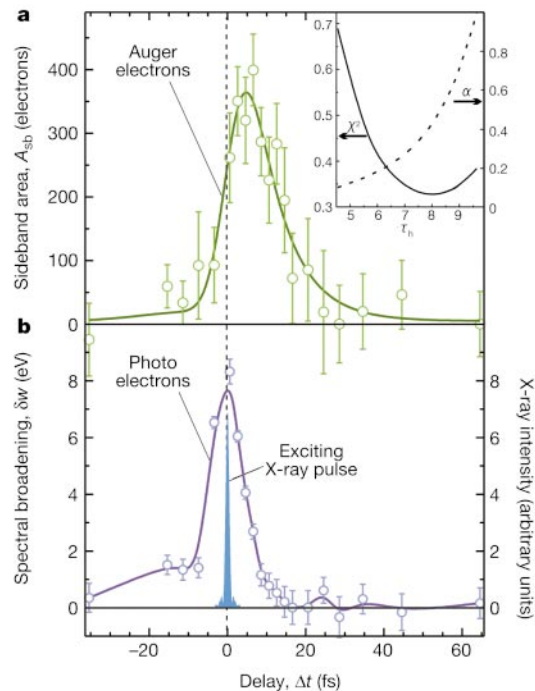
Figure 5 Probing the temporal evolution of Auger electron emission. **a**, Sideband area (circles) of the first-order sideband of the lowest-energy Kr $M_{4,5}N_1N_{2,3}$ Auger line extracted from the spectra of Fig. 4 and a fitted convolution of the exponential decay curve $R_0 \int \exp[-(t - t')/\tau_h]E_X^2(t')\,dt'$ with a power 2α of the amplitude envelope of the laser field. Because $\tau_X \ll \tau_L$, the latter is proportional to the spectral broadening of the $4p$ photoline from the same electron spectrum, presented in **b**. Panel **b** also displays the temporal intensity profile of the X-ray pulse computed from its measured energy distribution (FWHM ≈ 3 eV) assuming the absence of chirp, which applies to cut-off harmonic radiation under our experimental conditions as was verified in a recent experiment[5]. Inset, the confidence band for τ_h is confined by the merit function χ^2 and the valid range of α to $\tau_h = 7.9^{+1.0}_{-0.9}$ fs.

at the same instants. For $\tau_{el} \ll \tau_L$ and $\delta w(0)^2 \gg \Delta w(\infty)^2$, according to equation (1), the broadening displays the amplitude envelope $E_a(t)$ of the light field with the leading edge of the pulse being sampled at positive delays $\Delta t > 0$. A spline fit to the measured data (line in Fig. 5b) yields a FWHM duration of the field envelope $E_a(t)$ of slightly less than 10 fs, in excellent agreement with the result of a simultaneous autocorrelation measurement of the laser pulse ($\tau_L \approx 7$ fs). From $\delta w(\Delta t)$ we can also determine the start of the Auger emission ($\Delta t = 0$) with an accuracy of ± 0.5 fs.

In the low-intensity (perturbative) limit, the transition rate into the first-order sideband is proportional to the instantaneous laser intensity $E_a^2(t)$. However, for increasing intensities, depletion of the main peak and transition from the first-order into the second-order sideband causes deviation from this scaling. A modified scaling law of the form $E_a^{2\alpha}(t)$ with $0 < \alpha < 1$ represents a convenient approximation[16]. We confirmed the validity of this model for the relevant intensity range (10^{11}–10^{12} W cm^{-2}) experimentally by measuring A_{sb} as a function of the laser-pulse energy at a fixed delay Δt. We obtained $\alpha = 0.5 \pm 0.2$, in close agreement with previous findings[16] about the effective sublinear scaling of A_{sb} with laser intensity. We can now obtain quantitative dynamical information about the decay of the krypton M-shell vacancies by fitting the convolution of the Auger emission rate $R_0 \int \exp[-(t - t')/\tau_h] E_X^2(t') dt'$ and the effective sampling function $E_a^{2\alpha}(t - \Delta t)$ to the measured sideband area $A_{sb}(\Delta t)$. With $\Delta t = 0$ and $E_a(t)$ known from the photoelectron data and $E_X(t)$ estimated (Fig. 5b) to be gaussian with $\tau_X = 0.9$ fs, the only fit parameter that remains to be determined is the lifetime of the core hole, τ_h.

To double check the validity of our effective sampling function we have computed the best fit for several values of α between 0 and 1. The inset in Fig. 5a shows the optimum value of τ_h as a function of α along with the corresponding value of the merit function χ^2. The best-quality fit (represented by the line in Fig. 5a) has been obtained for $\alpha \approx 0.4$, which is within the above confidence interval acquired from an independent measurement. This analysis yields $\tau_h = 7.9^{+1.0}_{-0.9}$ fs for the lifetime of M($d_{5/2}$) vacancies in krypton. The measured lifetime yields an Auger linewidth of $\Gamma = \hbar/\tau_h = 84 \pm 10$ meV (not resolved by our spectrometer). This is in good accordance with 88 ± 4 meV, the result of recent energy-domain measurements[19]. The good agreement also indicates that post-collision interactions[21] have little, if any, influence on our time-resolved Auger spectra in spite of the near-threshold (97 eV) excitation.

Exploring atomic dynamics by time-domain studies

The exponential decay of krypton M-shell vacancies served as a benchmark process for testing the feasibility of time-resolved atomic inner-shell spectroscopy. The measured decay time can also be inferred from energy-domain measurements.

We believe we may nevertheless expect new insight into atomic dynamics from time-domain experiments. Whenever continuum states are involved in the atomic relaxation dynamics, several interfering relaxation pathways may connect the same initial and the same final state, resulting in a complex non-exponential temporal behaviour. For example, in the photoionization process, Fano-type[22] or shape[23] resonances are indicative of the outgoing electron being captured by its parent ion in a transient state for a short while. In the Auger process, post-collision interactions[21] tend to give rise to complications. Measuring the energy sweep and (non-exponential) envelope of the emitted electron wave packets with attosecond resolution will provide comprehensive insight into the transient states involved. Full exploration of the dynamical behaviour of multi-electron systems will therefore require time-domain

spectroscopy to complement energy-domain measurements.

Atomic inner-shell processes have so far been studied only in the absence of external perturbations (other than the particle initiating the process). However, in high-field interactions atoms are often exposed to light electric-field strengths comparable to that of the effective Coulomb fields acting on inner-shell electrons. Atoms exposed to atomic-scale light fields (relevant in, for example, X-ray laser research) may exhibit a dynamical behaviour significantly different from that of unperturbed atoms. Because of the short-lived optical perturbation this can be investigated exclusively by time-domain techniques.

The evolution of time-resolved atomic physics, what might be dubbed attophysics, and its impact on other fields will—beyond experimental advances—critically depend on progress in the theoretical understanding of the dynamics of excited multi-electron systems and their interaction with strong fields. □

1. Töpler, A. Vibroskopische Beobachtungen über die Schwingungsphasen singender Flammen (der chemischen Harmonica) mit Benutzung des Schlierenapparates. *Ann. Phys. Chem.* **128**, 126–139 (1866).
2. Zewail, A. Femtochemistry: atomic-scale dynamics of the chemical bond (adapted from the Nobel Lecture). *J. Phys. Chem. A* **104**, 5660–5694 (2000).
3. Bromage, J. & Stroud, C. R. Jr Excitation of three-dimensionally localized atomic electron wave packet. *Phys. Rev. Lett.* **83**, 4963–4966 (1999).
4. Drescher, M. *et al.* X-ray pulses approaching the attosecond frontier. *Science* **291**, 1923–1927 (2001) published online 15 February 2001; 10.1126/science.1058561.
5. Hentschel, M. *et al.* Attosecond metrology. *Nature* **414**, 509–513 (2001).
6. Papadogiannis, N. A., Witzel, B., Kalpouzos, C. & Charalambidis, D. Observation of attosecond light localization in higher order harmonic generation. *Phys. Rev. Lett.* **83**, 4289–4292 (1999).
7. Paul, P. *et al.* Observation of a train of attosecond pulses from high harmonic generation. *Science* **292**, 1689–1692 (2001).
8. Kienberger, R. *et al.* Steering attosecond electron wave packets with light. *Science* **297**, 1144–1148 (2002) published online 11 July 2002; 10.1126/science.1073866.
9. Krausz, F. Attosecond spectroscopy comes of age. *Opt. Photon. News* **13**, 62–68 (May 2002).
10. Krause, M. O. Atomic radiative and radiationless yields for K and L shells. *J. Phys. Chem. Ref. Data* **8**, 307–328 (1979).
11. Itatani, J. *et al.* Attosecond streak camera. *Phys. Rev. Lett.* **88**, 173903 (2002).
12. Kitzler, M., Milosevic, N., Scrinzi, A., Krausz, F. & Brabec, T. Quantum theory of attosecond XUV pulse measurement by laser-dressed photoionization. *Phys. Rev. Lett.* **88**, 173904 (2002).
13. Freeman, R. R. & Bucksbaum, P. H. Investigation of above-threshold ionization using subpicosecond pulses. *J. Phys. B* **24**, 325–347 (1991).
14. Schins, J. M. *et al.* Observation of laser-assisted Auger decay in argon. *Phys. Rev. Lett.* **73**, 2180–2183 (1994).
15. Glover, T. E., Schoenlein, R. W., Chin, A. H. & Shank, C. V. Observation of laser assisted photoelectric effect and femtosecond high order harmonic radiation. *Phys. Rev. Lett.* **76**, 2468–2471 (1996).
16. Bouhal, A. *et al.* Cross-correlation measurement of femtosecond noncollinear high-order harmonics. *J. Opt. Soc. Am. B* **14**, 950–956 (1997).
17. Aksela, H., Aksela, S. & Pulkkinen, H. Correlation effects in $4s^0 4p^6$ and $4s^1 4p^5$ configurations of krypton studied by the M-NN Auger decay. *Phys. Rev. A* **30**, 2456–2461 (1984).
18. Carlson, T. A. *et al.* Angular distribution of ejected electrons in resonant Auger processes of Ar, Kr, and Xe. *Phys. Rev. A* **39**, 1170–1185 (1988).
19. Jurvansuu, M., Kivimäki, A. & Aksela, S. Inherent lifetime widths of Ar $2p^{-1}$, Kr $3d^{-1}$, Xe $3d^{-1}$, and Xe $4d^{-1}$ states. *Phys. Rev. A* **64**, 012502 (2001).
20. Schmidtke, B. *et al.* The Kr $M_{4,5}N_1N_{2,3}$ ($^1P_1$) Auger decay: measurement of the transferred spin polarization and analysis of Auger amplitudes. *J. Phys. B* **34**, 4293–4310 (2001).
21. Borst, M. & Schmidt, V. Vanishing postcollision interaction in inner-shell photoionization. *Phys. Rev. A* **33**, 4456–4458 (1986).
22. Fano, U. Effects of configuration interaction on intensities and phase shifts. *Phys. Rev.* **124**, 1866–1878 (1961).
23. Becker, U. *et al.* Subshell photoionization of Xe between 40 and 1000 eV. *Phys. Rev. A* **39**, 3902–3911 (1989).

Correspondence and requests for materials should be addressed to M.D. (e-mail: drescher@physik.uni-bielefeld.de) or F.K. (e-mail: ferenc.krausz@tuwien.ac.at).